JOURNAL OF THERMOPHYSICS AND HEAT TRANSFER
Vol. 15, No. 4, October–December 2001

Drag Model for Free Molecule Flow

John F. Belena* and Z. U. A. Warsi†
Mississippi State University, Mississippi State, Mississippi 39762

A new drag model for convex surfaces engaged in free molecule flow has been developed under the condition of surface adsorption equilibrium using the hard cube model of atom scattering and the surface fractional coverage involved in gas adsorption. The new differential surface element drag and lift equations are only valid when the mass ratio of gas molecule to surface molecule is less than unity.

Nomenclature

b	=	average gas emission speed divided by speed of flight
C_{p_s}	=	heat capacity of surface material
$d\boldsymbol{D}$	=	differential drag force
$d\boldsymbol{L}$	=	differential lift force
E_a^i	=	activation energy for adsorption of chemical gas species i
f_{ga}	=	total global species fraction of gas stream adsorbed
f_{ga_i}	=	total global fraction of species i gas adsorbed
$G(V_s)$	=	surface molecule probability density
h	=	Planck's constant (6.6262×10^{-34} J-s)
$\boldsymbol{i}$	=	unit vector in x direction
J	=	Jacobian
$J\,\mathrm{d}\xi\,\mathrm{d}\eta$	=	differential surface area element
J_i	=	surface incident mass flux of chemical gas species i
k	=	Boltzmann constant (1.381×10^{-23} J/k)
$k_{(\cdot)}$	=	gas rate constant for adsorption in collision mode $(\cdot)$
$\hat{\boldsymbol{L}}$	=	unit vector in the direction of aerodynamic lift
$\dot{m}_d$	=	diffusive gas mass rate
m_g	=	mass of gas molecule
$\dot{m}_i$	=	incident gas mass rate
m_s	=	mass of surface molecule
$\dot{m}_s$	=	scattered gas mass rate
$\hat{\boldsymbol{n}}$	=	surface normal vector
nc	=	number of collision types comprising a collision scenario
P	=	species gas pressure
$P_{(\cdot)}$	=	collision mode probability nonnormalized
q_r	=	square root of the dot product of the exit stream velocity
$q_{s(\cdot)}$	=	square root of the dot product of the surface molecule velocity
R_g	=	gas constant
$r_{(\cdot)}$	=	gas rate constant for desorption in collision mode $(\cdot)$
$S_{\text{gn}}(\hat{\boldsymbol{L}} \cdot \hat{\boldsymbol{n}})$	=	value is $+1$ if $\hat{\boldsymbol{L}} \cdot \hat{\boldsymbol{n}} \geq 0$ and -1 if $\hat{\boldsymbol{L}} \cdot \hat{\boldsymbol{n}} < 0$
S_i, S	=	species incident molecular speed ratio
$S_{i\text{o}}$	=	adsorbed mass flux
$SP_n(\theta_r)_{(\cdot)}$	=	species normalized scattering probability distribution
T_g	=	gas temperature
T_{rm}	=	gas reduction method exit gas temperature
T_s	=	surface temperature
V_i	=	incident gas stream speed
$\boldsymbol{V}_i$	=	incident gas stream velocity
$VP_n(V_r \mid \theta_r)_{(\cdot)}$	=	species normalized velocity probability distribution for gas scattered at angle θ_r
V_r	=	scattered gas speed
$\boldsymbol{V}_r$	=	scattered gas velocity
V_r^*	=	gas molecule minimum surface escape speed
$\hat{\boldsymbol{V}}_r$	=	unit vector in scattered gas directions
$\hat{V}_{r_{(\cdot)}}$	=	most probable scattering gas speed
$\bar{V}_{r_{(\cdot)}}$	=	mean scattering gas speed
$V_{\text{rms}_{(\cdot)}}$	=	rms scattering gas speed
V_{rm}	=	gas reduction method scattering exit speed
V_s	=	surface molecule speed, $\sqrt{[m_s/(2kT_s)]}$
$\boldsymbol{V}_s$	=	surface molecule velocity
W	=	nondimensional surface trapping potential well depth
W_c	=	factor in the expression for $VP_n(V_r \mid \theta_r)_{(\cdot)}$
w_c	=	thermal speed of surface molecules
α_x	=	rotation deviation in x direction of surface from flat in radians
α_y	=	rotation deviation in y direction of surface from flat in radians
$\Delta\Lambda$	=	phase range of surface molecule inside its box
$\Delta\Lambda_{(\cdot)}$	=	collision mode phase angle range
$\delta_{(\cdot)}$	=	factor in the expression for $SP_n(\theta_r)_{(\cdot)}$, $VP_n(V_r \mid \theta_r)_{(\cdot)}$
η	=	surface coordinate
η_c	=	factor in $VP_n(V_r \mid \theta_r)_{(\cdot)}$
θ_c	=	cone semivertex angle
θ_i	=	incident angle to surface normal of incoming gas stream
θ_r	=	gas scattering angle
θ_{rm}	=	gas reduction method scattering exit angle
$\theta_{r_{\text{nsc}}}$	=	location of nonsmooth behavior for $SP_n(\theta_r)_{(\cdot)}$
$\theta_{r_{\text{rms}(\cdot)}}$	=	rms gas scattering angle
$\bar{\theta}_{r(\cdot)}$	=	mean gas scattering angle
$\hat{\theta}_{r(\cdot)}$	=	most probable gas scattering angle
Λ	=	phase angle of surface molecule inside its box
λ	=	lambda collision criteria
μ_g	=	mass ratio of gas molecule to surface molecule
$\mu_{i\text{o}}$	=	saturation adsorption coefficient of chemical gas species i
ξ	=	surface coordinate
ρ	=	incident gas stream density
ρ_d	=	diffusive gas mass density
ρ_i	=	incident gas mass density
ρ_s	=	scattered gas mass density
σ_c	=	factor in $VP_n(V_r \mid \theta_r)_{(\cdot)}$
$\Phi_{(\cdot)}$	=	percent of surface involved in adsorption in collision mode $(\cdot)$
$\phi_{(\cdot)}$	=	factor in the expression for $SP_n(\theta_r)_{(\cdot)}$, $VP_n(V_r \mid \theta_r)_{(\cdot)}$
$\psi_{(\cdot)}$	=	collision mode probability
$(\cdot)$	=	collision mode

Received 28 March 2001; revision received 28 June 2001; accepted for publication 29 June 2001.

*Researcher, Department of Aerospace Engineering.
†Professor, Department of Aerospace Engineering.

Introduction

THIS paper is concerned with presenting a new methodology for the calculation of drag and lift on an aerobody with a convex surface in hypersonic rarefied flow in gases of extremely low density (i.e., free molecule flow). Historically, the forces of drag and lift have been calculated using the tangential and normal surface accommodation coefficients as originally suggested by Maxwell.[1] For all possible gas-surface combinations in hypersonic rarefied flows, many have no experimental data readily available in the open literature that would provide the normal and tangential surface accommodation coefficients. The method for calculating aerodynamic forces presented in this paper provides an alternative to the use of surface accommodation coefficients. An observer on a transatmospheric vehicle or on an Earth satellite would regard the atmosphere through which he is moving as being approximately a monoenergetic beam of kinetic energy range 100–0.50 eV because the speeds of travel are very much higher than the mean gas speeds. At these hypersonic speeds of travel, the spatial distribution of the air particles reemitted by various engineering surfaces displays the typical forward lobular distribution with little if any backscattering.[2] With an eye on engineering and numerical computational simplicity, there is a classical mechanics model, the "hard-cube" model,[3–6] whose behavior agrees qualitatively with experimental data for scattering of a monoenergetic beam of gas particles from a solid surface for the kinetic energies of interest. The principal objective of this study is to build a drag model for convex surfaces in hypersonic free molecule flow based on the scattering characteristics of the hard-cube model where surface adsorption and reemission appear explicitly.

Gas–Solid Model

In the case of a gas flowing past a solid body, the boundary conditions describe the interaction of the gas molecules with the solid walls. It is to this gas-surface interaction that one can trace the origin of the drag and lift exerted by the gas on the body. When a molecule interacts with a surface, it is adsorbed and can dissociate, form chemical bonds, become ionized, or even displace surface molecules and cause sputtering. The state of the surface layer depends on the surface roughness and cleanliness. In general, adsorbed layers are present, and the interaction of a given gas molecule with the surface also depends on the distribution of molecules incident on the surface. When considering the impact of a gas molecule with a surface, three possible outcomes can occur as shown in Fig. 1.

In most gas-surface interactions of aerodynamic interest, all three impact outcomes are in operation as an aerospace vehicle encounters free molecule flow.

In the drag model the hard-cub model will provide the elastic collision and direct inelastic collision scattering outcomes. The trapping-desorption collisions are handled through the modeling of the diffusive efflux. In general, for hypersonic free molecule flow the calculation of drag and lift will involve outcome scenarios where the three possible gas-surface collision types will occur.

The hard-cube molecular model is built around the following four criteria:

1) The gas molecule and the surface molecule are considered as rigid elastic particles. This implies that the intermolecular potential

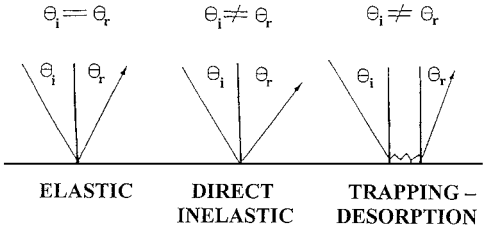

Fig. 1 Possible outcomes of the collision of a gas atom with a surface. Elastic: low temperature; weak interaction; light molecule; energetically smooth, regular surface. Direct inelastic: higher temperature; weak interaction; heavier molecule; energetically rough, irregular surface. Trapping-desorption: low temperature, strong interaction, heavier molecule.[7]

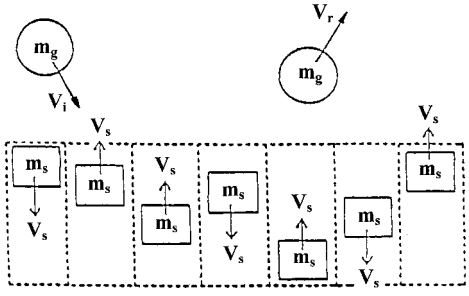

Fig. 2 Gas–solid interaction system.

between the gas molecule and the surface is such that the repulsive force is impulsive.

2) Collisions between the gas molecule and the surface do not change the tangential component of the velocity of the gas molecule because there are no forces acting parallel to the surface; the surface is perfectly smooth. When a gas molecule collides with the surface, the normal component of velocity to the surface changes according to the laws for collision of rigid elastic bodies.

3) The surface molecules are represented by independent cubes confined by square well potentials. A gas molecule interacts with a single surface molecule by entering the surface molecule's square well potential, colliding with the surface molecule and then departing.

4) A one-dimensional Maxwellian distribution function is assigned for the component of velocity of the surface molecules normal to the surface.

In our model of the gas-solid interaction system, we consider the surface to be an ensemble of hard cubes each bound to move along the surface normal direction within a one-dimensional box with a Maxwellian distribution of velocities V_s as shown in Fig. 2. The one-dimensional boxes are held rigid and are impermeable to the hard cube molecules. The hard cube molecules move freely between the ends of their respective boxes with constant speed. The entire gas–solid interaction is confined to the inside of the box, and when the interaction is completed the gas molecule emerges from the box with an exit velocity V_r, leaving the solid surface molecule reflecting between the end walls of its box with speed V_s.

With an eye on validating the gas–solid system for high temperatures and low-density environments such as encountered by an aerospace reentry vehicle, we turn to the definition of a perfect classical gas. For a gas consisting of molecules moving about freely in space, the molecules are separated far from each other and interact only very weakly. At any instant of time, only a very small fraction of the gas molecules are engaged in a strong interaction, that is, are colliding. The perfect gas representation views the potential energy of interaction between the gas molecules as negligible compared to their kinetic energy of motion. With negligible interaction energy and using concepts from statistical mechanics, we can obtain an expression that says that our gas–solid interaction system is valid as long as the stream gas density ρ and the stream gas temperature T_g are related as

$$(\rho/m_g)\cdot\left[h^2/(2\pi m_g k T_g)\right]^{\frac{3}{2}} \ll 1 \qquad (1)$$

Equation (1) states that if the gas stream temperature is sufficiently high and the gas stream density sufficiently low, the gas molecules will interact as localized wave packets according to the classical hard-cube molecular interaction model. Equation (1) is valid even in the continuum region.

Collision Environments

To describe the different types of collisions possible during the gas-surface interaction, we can describe the gas–solid system at the instant before the collision by a symbol of the type $(\downarrow\atop\uparrow)$, where the top arrow indicates the direction of travel normal to the surface of the gas molecule and the bottom arrow indicates the direction of travel normal to the surface of the surface molecule. For the case of

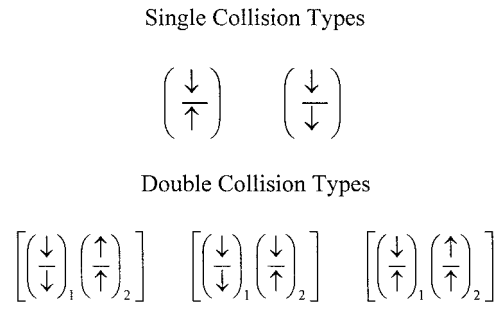

Fig. 3 Collision types for $\mu_g < 1$.

$\mu_g > 1$, the gas molecule can involve any number of collisions on the surface. An exact solution of the general problem for any value of μ_g is at present intractable, and we will develop our drag model based on $\mu_g < 1$.

For the case of $\mu_g < 1$, there are five distinct types of collision possible: two single-collision types and three double-collision types.[3] The collision sequence in the double-collision types is provided by the numerical subscripts as shown in Fig. 3. For the double-collision types collisions 1, 2 are occurring in the same location on the surface.

With V_{in} the normal speed component of the incoming gas particle and V_s the speed of the surface molecule inside its rigid box and letting V_{in}, V_s be positive quantities, we have the following collision relations, which are derived using perfectly elastic one-dimensional collision theory[7]:

Single-collision types:

$$\left(\frac{\downarrow}{\uparrow}\right)(1+\mu_g)V_{\text{rn}} = (1-\mu_g)V_{\text{in}} + 2V_s$$

$$\left(\frac{\downarrow}{\downarrow}\right)(1+\mu_g)V_{\text{rn}} = (1-\mu_g)V_{\text{in}} - 2V_s$$

Double-collision types:

$$\left[\left(\frac{\downarrow}{\downarrow}\right)_1\left(\frac{\uparrow}{\uparrow}\right)_2\right]\left[\left(\frac{\downarrow}{\downarrow}\right)_1\left(\frac{\downarrow}{\uparrow}\right)_2\right](1+\mu_g)^2 V_{\text{rn}}$$
$$= 4(1-\mu_g)V_s - \left(1-6\mu_g+\mu_g^2\right)V_{\text{in}}$$

$$\left[\left(\frac{\downarrow}{\uparrow}\right)_1\left(\frac{\uparrow}{\uparrow}\right)_2\right](1+\mu_g)^2 V_{\text{rn}} = -4(1-\mu_g)V_s$$
$$-\left(1-6\mu_g+\mu_g^2\right)V_{\text{in}}$$

To determine the collision scenario as shown in Tables A1–A3 in Appendix A, we must use an index collision,[3] which is represented by the ratio of gas molecule speed to surface molecule speed in the surface normal direction. The index collision is used to characterize the collision scenario occurring on the surface. In this paper the representative index collision used to characterize the gas-surface interaction is the ratio of mean gas molecule speed to mean surface molecule speed called the lambda collision criteria.

$$\lambda = \overline{\boldsymbol{V}_i \cdot \hat{\boldsymbol{n}}}/\bar{V}_s \tag{2}$$

For a large freestream Mach number we concern ourselves only with the streaming gas velocity, and we use the lambda collision criteria[8] to determine the types of collisions taking place on the surface where

$$\lambda = \frac{R_g T_g}{2\pi C_{p_s} T_s}\left\{\exp\left[-(S_i\cos\theta_i)^2\right]\right.$$
$$\left.+\sqrt{\pi}(S_i\cos\theta_i)(1+\operatorname{erf}[S_i\cos\theta_i])\right\}^2$$

For $0 < \mu_g < 1$ there are 12 collision scenarios as shown in Tables A1–A3 in Appendix A.

Collision Probabilities

In our gas–solid interaction system the surface molecule is constrained to move up and down in its box in the surface normal direction. To calculate the collision probabilities, we need to define the phase angle Λ of the surface molecule as it cycles in its box. At the instant the surface molecule is at the top of its box, its phase is $\Lambda = 0$; after it travels downward the instance that it arrives at the bottom of its box its phase is $\Lambda = \pi$; after it travels upward the instance before it arrives at the top of the box its phase is $\Lambda = 2\pi$; the intermediate phases are defined by letting Λ vary linearly with the position of the surface molecule in its box. Thus, Λ is restricted to lie between 0 and 2π. The description of the collisions that occur for all possible values of λ and Λ for $0 < \mu_g < 1$ are given in Tables B1 and B2 in Appendix B.

Assuming thermal equilibrium for the surface molecules and using the phase angle range $\Delta\Lambda_{(\cdot)}$ for each collision type, we can easily find the probability integral for each collision mode as given by

$$P_{(\cdot)} = \int_0^{V_{\text{in}}} G(V_s)\left[\left(\frac{\Delta\Lambda_{(\cdot)}}{2\pi}\right)\right]\mathrm{d}V_s$$

$$G(V_s) = \left(\frac{2w_c}{\sqrt{\pi}}\right)\exp\left(-w_c^2 V_s^2\right), \qquad w_c^2 = \frac{m_s}{2kT_s}$$

$(\cdot) \equiv$ collision modes

$$(\cdot) \in \left\{\left(\frac{\downarrow}{\uparrow}\right), \left(\frac{\downarrow}{\downarrow}\right), \left[\left(\frac{\downarrow}{\downarrow}\right)_1\left(\frac{\uparrow}{\uparrow}\right)_2\right],\right.$$
$$\left.\left[\left(\frac{\downarrow}{\downarrow}\right)_1\left(\frac{\downarrow}{\uparrow}\right)_2\right], \left[\left(\frac{\downarrow}{\uparrow}\right)_1\left(\frac{\uparrow}{\uparrow}\right)_2\right]\right\}$$

In each of the collision scenarios I–XII in Tables B1 and B2 in Appendix B, the gas-surface collision mode probabilities $\psi_{(\cdot)}$ are found according to

$$\psi_{(\cdot)} = P_{(\cdot)} \Big/ \left(\sum_{(\cdot)} P_{(\cdot)}\right)$$

Scattering Velocity

To calculate the scattering velocity of the gas stream leaving the surface, we use the normalized scattering probability and exit speed probability distribution for each collision mode occurring on the surface. To determine the scattering angle $\theta_{r_{(\cdot)}}$ from the surface normal, we use the scattering probability distribution[8] given by

$$SP_n(\theta_r)_{(\cdot)} = \frac{\delta_{(\cdot)} \Big/ \phi_{(\cdot)}^{\frac{5}{2}}}{\int_0^{\pi/2}\left(\delta_{(\cdot)} \Big/ \phi_{(\cdot)}^{\frac{5}{2}}\right)\mathrm{d}\theta_r} \tag{3}$$

The $\delta_{(\cdot)}$, $\phi_{(\cdot)}$ expressions for each collision type are provided in Appendix C.

There are three exit gas scattering angles of interest determined from the scattering probability distribution Eq. (3) that can be used in the calculation of drag and lift as follows:

$\hat{\theta}_{r_{(\cdot)}} \equiv$ the most probable exit angle $\theta_{r_{(\cdot)}}$

$$\hat{\theta}_{r(\cdot)} = \left[SP_n(\theta_r)_{(\cdot)}\right]_{\max}, \qquad \bar{\theta}_{r_{(\cdot)}} \equiv \text{the mean exit angle } \theta_{r_{(\cdot)}}$$

$$\bar{\theta}_{r_{(\cdot)}} = \int_0^{\pi/2} \theta_r\left[SP_n(\theta_r)_{(\cdot)}\right]\mathrm{d}\theta_r, \qquad \theta_{r_{\text{rms}(\cdot)}} \equiv \text{the rms exit angle } \theta_{r_{(\cdot)}}$$

$$\theta_{r_{\text{rms}(\cdot)}} = \left[\int_0^{\pi/2} \theta_r^2\left[SP_n(\theta_r)_{(\cdot)}\right]\mathrm{d}\theta_r\right]^{\frac{1}{2}}$$

$$(\cdot) \in \left\{ \left(\begin{matrix}\downarrow\\ \uparrow\end{matrix}\right), \left(\begin{matrix}\downarrow\\ \downarrow\end{matrix}\right), \left[\left(\begin{matrix}\downarrow\\ \downarrow\end{matrix}\right)_1 \left(\begin{matrix}\uparrow\\ \uparrow\end{matrix}\right)_2\right], \left[\left(\begin{matrix}\downarrow\\ \downarrow\end{matrix}\right)_1 \left(\begin{matrix}\downarrow\\ \uparrow\end{matrix}\right)_2\right], \left[\left(\begin{matrix}\downarrow\\ \uparrow\end{matrix}\right)_1 \left(\begin{matrix}\uparrow\\ \uparrow\end{matrix}\right)_2\right] \right\} \tag{4}$$

With the velocity probability distribution and the normalized collision probability $\psi_{(\cdot)}$ known for each collision mode occurring on the surface for the purpose of drag and lift, we postulate to characterize the exit gas stream with a scattering speed V_r given by

$$V_r = \sqrt{\left[\left(\sum_{(\cdot)} V_{r_{(\cdot)}} \psi_{(\cdot)} \cos\theta r_{(\cdot)}\right)^2 + \left(\sum_{(\cdot)} V_{r_{(\cdot)}} \psi_{(\cdot)} \sin\theta r_{(\cdot)}\right)^2\right] \Big/ nc}$$

The scattering probability distributions will display nonsmooth behavior at the following exit angles θr_{ns}:

$$\left(\begin{matrix}\downarrow\\ \uparrow\end{matrix}\right), \left(\begin{matrix}\downarrow\\ \downarrow\end{matrix}\right): \theta r_{\text{ns}} = \tan^{-1}\left[\left(\frac{1+\mu_g}{1-\mu_g}\right)\tan\theta_i\right]$$

$$\left[\left(\begin{matrix}\downarrow\\ \downarrow\end{matrix}\right)_1 \left(\begin{matrix}\uparrow\\ \uparrow\end{matrix}\right)_2\right], \left[\left(\begin{matrix}\downarrow\\ \downarrow\end{matrix}\right)_1 \left(\begin{matrix}\downarrow\\ \uparrow\end{matrix}\right)_2\right], \left[\left(\begin{matrix}\downarrow\\ \uparrow\end{matrix}\right)_1 \left(\begin{matrix}\uparrow\\ \uparrow\end{matrix}\right)_2\right]:$$

$$\theta r_{\text{ns}} = \tan^{-1}\left[-\frac{(1+\mu_g)^2}{\left(1-6\mu_g+\mu_g^2\right)}\tan\theta_i\right]$$

With the certainty that the gas molecule will scatter off the surface somewhere in the range of $0\,\text{deg} \le \theta_r \le 90\,\text{deg}$, the integral of the scattering probability distribution $SP_n(\theta_r)_{(\cdot)}$ from $0\,\text{deg} \le \theta_r \le 90\,\text{deg}$ equals 1. The values of $S_{(\cdot)}/\phi_{(\cdot)}^{5/2}$ are such that the distribution $SP_n(\theta_r)_{(\cdot)}$ will have values of $SP_n(\theta_r)_{(\cdot)} > 1$.

With a scattering exit angle from the surface normal $\theta_{r_{(\cdot)}}$ known, the velocity probability distribution[8] of the scattered gas is given by

$$VP_n(V_r \mid \theta_r)_{(\cdot)} = \frac{W_{c_{(\cdot)}} \phi_{(\cdot)}^{\frac{5}{2}} \exp\left\{-\sigma_{c_{(\cdot)}}\right\}}{\delta_{(\cdot)} \int_0^\infty W_{c(\cdot)} \delta_{(\cdot)}^{-1} \phi_{(\cdot)}^{\frac{5}{2}} \exp\left\{-\sigma_{c_{(\cdot)}}\right\} \mathrm{d}q_r} \tag{5}$$

where

$$\chi(S_i, \theta_i) = \left\{\exp\left[-(S_i\cos\theta_i)^2\right] + \sqrt{\pi}(S_i\cos\theta_i)(1+\operatorname{erf}[S_i\cos\theta_i])\right\}$$

$$q_s = \sqrt{\boldsymbol{V}_s \cdot \boldsymbol{V}_s}, \qquad q_r = \sqrt{\boldsymbol{V}_r \cdot \boldsymbol{V}_r}$$

$$W_{c_{(\cdot)}} = \frac{8\chi(S_i, \theta_i)}{3\pi}\eta_{c_{(\cdot)}}\sqrt{\frac{R_g T_g}{2}}\left(\frac{\sin\theta_r}{\sin\theta_i}\right)$$

$$\eta_{c_{(\cdot)}} = q_r\left|\frac{\partial q_{s_{(\cdot)}}}{\partial\theta_r}\right|\frac{4\pi}{\chi(S_i,\theta_i)}\left(\frac{m_g}{2\pi k T_s}\right)^{\frac{3}{2}}\left(\frac{m_s}{2\pi k T_s}\right)^{\frac{1}{2}} \times \left(\frac{[q_r\cot\theta_i\sin\theta_r]^2}{\cos^3\theta_i}\right) \tag{6}$$

$$\sigma_{c(\cdot)} = \left(\frac{m_g}{2kT_g}\right)\left[\frac{q_r\cot\theta_i\sin\theta_r}{\cos\theta_i}\right]^2 + \left(\frac{m_s}{2kT_s}\right)q_s^2 \tag{7}$$

$\delta_{(\cdot)}, \phi_{(\cdot)} =$ Eqs. (C1–C8) in Appendix C

The expressions for $q_{s(\cdot)}$ used in Eqs. (6) and (7) are given in Appendix C for the five collision types.

There are three exit gas scattering speeds of interest determined from the velocity distribution function (5) that we can use in the calculation of drag and lift as follows:

$\hat{V}_{r_{(\cdot)}} \equiv$ the most probable exit speed $V_{r_{(\cdot)}}$ at angle $\theta_{r_{(\cdot)}}$

$$\hat{V}_{r(\cdot)} = \left[VP_n(V_r \mid \theta_r)_{(\cdot)}\right]_{\max}$$

$\bar{V}_{r_{(\cdot)}} \equiv$ the mean exit speed $V_{r_{(\cdot)}}$ at exit angle $\theta_{r_{(\cdot)}}$

$$\bar{V}_{r(\cdot)} = \int_0^\infty V_r\left[VP_n(V_r \mid \theta_r)_{(\cdot)}\right]\mathrm{d}V_r$$

$V_{r_{\text{rm}(\cdot)}} \equiv$ the rms exit speed $V_{r_{(\cdot)}}$ at exit angle $\theta_{r_{(\cdot)}}$

$$V_{r_{\text{rms}(\cdot)}} = \left[\int_0^\infty V_r^2\left[VP_n(V_r \mid \theta_r)_{(\cdot)}\right]\mathrm{d}V_r\right]^{\frac{1}{2}}$$

Random Emission Velocity

In calculating the aerodynamic drag and lift component caused by random emission,[9] we use a characteristic velocity normal to the surface, the average emission velocity vector. The net velocity component in the surface normal direction for all molecules emitted in a unit hemisphere above a differential surface area is given by

$$\tfrac{1}{2} b V_i \hat{\boldsymbol{n}}$$

The average speed of emission is given by bV_i, where $b(S_i, V_r^*, T_s)$ and V_i is the speed of the gas stream relative to the surface in flight. With a Maxwellian velocity distribution for the re-emitted molecules and knowledge of V_r^*, we can find the expressions for the constant b and the average speed bV_i.

$$b = \frac{2}{S_i\sqrt{\pi}}\left(\sqrt{\frac{T_s}{T_g}} + \frac{V_r^*}{\sqrt{2R_g T_g}}\right)\exp\left\{-\frac{V_r^*}{\sqrt{2R_g T_s}}\right\}$$

$$S_i = \frac{V_i}{\sqrt{2R_g T_g}}, \qquad bV_i = \frac{2}{\sqrt{\pi}}\left(\sqrt{2R_g T_s} + V_r^*\right)\exp\left\{-\frac{V_r^*}{\sqrt{2R_g T_s}}\right\}$$

where the minimum gas molecule exit speed V_r^* at $\theta_r = 0$ deg is given by

$$V_r^* = \frac{\sqrt{W 2R_g T_g}}{\cos(\phi)\cos(\alpha_y)\cos(\alpha_x) + \sin(\phi)\sin(\alpha_y)}$$

where W is the nondimensional surface trapping potential well depth and rotation angles α_x, α_y provide a measure of the deviation from a flat surface as shown in Fig. 4.

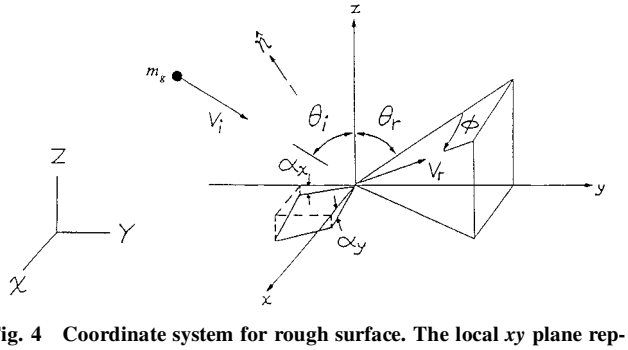

Fig. 4 Coordinate system for rough surface. The local *xy* plane represents the ideal flat surface, and $\hat{n}$ represents the normal to the actual rough surface at the origin.

Gas Adsorption

When gases are in contact with solid surfaces, in most cases the concentration of gas at the surface is greater than its value away from the surface.[10] As the gas molecules become attached to the solid surface, the attractive force of the solid surface becomes partially neutralized, and at equilibrium the attractive force of the solid surface acquires its minimum value for the given thermodynamic state of the gas–solid system. The physical phenomena by which the gas molecules become attached or trapped on the solid surface is called adsorption. There is basically two kinds of adsorption processes, physical adsorption and chemisorption, which are distinguished from each other depending upon the nature of the binding forces between the molecules of the gas and solid. Physical adsorption is caused by the weak forces of polarization interaction between the gas and surface molecules. The binding between the gas and the surface molecules is such that there is no sharing or transfer of electrons, and, therefore, the physical and chemical properties of the gas-solid system are not altered.[11] Physical adsorption does not require an activation energy, and it is a fast process at whatever temperature it occurs. Chemisorption involves the sharing or transference of electrons between the gas molecule and the surface molecule leading to chemical bonding, which satisfies the electron valency requirement of the surface. Chemisorption may require an activation energy and high heats of adsorption.

In general, both physical and chemical adsorption take place simultaneously. Surface adsorption initially begins with chemisorption, and as the amount of the adsorbed gas increases the mechanism of adsorption gradually changes to physical adsorption. In the case of high-speed free molecule flow where only a portion of the surface area at any given time is involved in the adsorption process, chemisorption will most likely be the dominant adsorption process. In the study of surfaces exposed to fluid flows,[12] an estimate of the adsorbed fraction of the incident gas stream to the surface f_{ga_i} appears in a quantity of interest called "surface incident adsorbed mass flux" S_{io} given by

$$S_{\mathrm{io}} = \mu_{\mathrm{io}} \exp\left\{-E_a^i \big/ kT_g\right\} J_i, \qquad S_{\mathrm{io}} = f_{\mathrm{ga}_i} J_i$$

For equilibrium flow we use the Langmuir model[13] of the adsorption process modified to include the collision modes. The Langmuir model assumes that adatoms are held on specific sites on the surface such that there is no motion of the atoms over the surface. In the Langmuir model the only effect the presence of one adatom has on any other gas atom is that the gas atoms striking the surface site that is already occupied do not adsorb. In the Langmuir model the gas molecule uptake is limited to a monolayer. The Langmuir model provides a good description of the adsorption process in many real systems and especially in systems in which strong chemisorption occurs.

Adsorption is an exothermic process and the energy released generally heats the adsorbent surface. For gas molecules that do not dissociate on being adsorbed, the Langmuir equation for a pure gas species can be written as

$$r_{(\cdot)}\Phi_{(\cdot)} = k_{(\cdot)}\left(1 - \Phi_{(\cdot)}\right) P \psi_{(\cdot)}$$

The Langmuir equation for dissociative adsorption of a pure gas species is written as

$$r_{(\cdot)}\Phi_{(\cdot)}^2 = k_{(\cdot)}\left(1 - \Phi_{(\cdot)}\right)^2 P \psi_{(\cdot)}$$

where

$$(\cdot) \in \left\{ \left(\begin{matrix}\downarrow\\ \uparrow\end{matrix}\right), \left(\begin{matrix}\downarrow\\ \downarrow\end{matrix}\right), \left[\left(\begin{matrix}\downarrow\\ \downarrow\end{matrix}\right)_1 \left(\begin{matrix}\uparrow\\ \uparrow\end{matrix}\right)_2\right], \left[\left(\begin{matrix}\downarrow\\ \downarrow\end{matrix}\right)_1 \left(\begin{matrix}\downarrow\\ \uparrow\end{matrix}\right)_2\right], \left[\left(\begin{matrix}\downarrow\\ \uparrow\end{matrix}\right)_1 \left(\begin{matrix}\uparrow\\ \uparrow\end{matrix}\right)_2\right] \right\}$$

Surface Mass Rates

For the condition of adsorption equilibrium in steady flow, the law of conservation of mass requires that the rate of mass incident on the surface be equal to the rate of mass leaving the surface caused by scattering and desorption as given by

$$\frac{\mathrm{d}\dot{m}_i}{\mathrm{d}A} = \frac{\mathrm{d}\dot{m}_s}{\mathrm{d}A} + \frac{\mathrm{d}\dot{m}_d}{\mathrm{d}A} \tag{8}$$

when $\boldsymbol{V}_i \cdot \hat{\boldsymbol{n}} < 0$, the incoming mass flux is given by

$$\frac{\mathrm{d}\dot{m}_i}{\mathrm{d}A} = -\rho_i (\boldsymbol{V}_i \cdot \hat{\boldsymbol{n}}) \tag{9}$$

The exit scattered mass flux from the surface is given by

$$\frac{\mathrm{d}\dot{m}_s}{\mathrm{d}A} = \rho_s (\boldsymbol{V}_r \cdot \hat{\boldsymbol{n}})(1 - \Phi), \qquad \Phi \le 1 \tag{10}$$

Integrating the velocity distribution of the adsorbed gas molecules gives the diffusive mass flux as

$$\frac{\mathrm{d}\dot{m}_d}{\mathrm{d}A} = \rho_d \sqrt{\frac{R_g T_s}{2\pi}} \exp\left\{-\frac{V_r^{*2}}{2R_g T_s}\right\} \Phi, \qquad \Phi \le 1 \tag{11}$$

Introducing Eqs. (9–11) into the continuity Eq. (8), we get when $\boldsymbol{V}_i \cdot \hat{\boldsymbol{n}} < 0$

$$-\rho_i (\boldsymbol{V}_i \cdot \hat{\boldsymbol{n}}) = \rho_s (\boldsymbol{V}_r \cdot \hat{\boldsymbol{n}})(1 - \Phi) + \rho_d \sqrt{\frac{R_g T_s}{2\pi}} \exp\left\{-\frac{V_r^{*2}}{2R_g T_s}\right\} \Phi$$

$$\rho_s = \frac{-\rho_i (\boldsymbol{V}_i \cdot \hat{\boldsymbol{n}})(1 - f_{\mathrm{ga}})}{(\boldsymbol{V}_r \cdot \hat{\boldsymbol{n}})(1 - \Phi)}$$

$$\rho_d = \frac{-\rho_i (\boldsymbol{V}_i \cdot \hat{\boldsymbol{n}})(f_{\mathrm{ga}})}{\sqrt{(R_g T_s / 2\pi)} \exp\left(-V_r^{*2} \big/ 2R_g T_s\right) \Phi}$$

Differential Surface Element Drag and Lift

The drag equation for a differential surface element is given by

$$d\boldsymbol{D} = \left(\mathrm{d}\dot{m}_i V_i - \mathrm{d}\dot{m}_s \left[\boldsymbol{V}_r \cdot \frac{\boldsymbol{V}_i}{V_i}\right] - \mathrm{d}\dot{m}_d \left[\frac{b}{2} V_i \hat{\boldsymbol{n}} \cdot \frac{\boldsymbol{V}_i}{V_i}\right] \right) \left[\frac{\boldsymbol{V}_i}{V_i}\right]$$

When $\boldsymbol{V}_i \cdot \hat{\boldsymbol{n}} < 0$ and $V_{r_{(\cdot)}} \cdot \psi_{(\cdot)} \le V_i$, then

$$d\boldsymbol{D} = \left(-\rho_i V_i (\boldsymbol{V}_i \cdot \hat{\boldsymbol{n}}) - \rho_s \left[\sum_{(\cdot)} \left(\boldsymbol{V}_{r_{(\cdot)}} \cdot \hat{\boldsymbol{n}}\right) \psi_{(\cdot)} \right] (1 - \Phi) \right.$$

$$\times \left\{ \frac{\sum_{(\cdot)} \left[\left(\boldsymbol{V}_{r_{(\cdot)}} \cdot \boldsymbol{V}_i / V_i\right) \psi_{(\cdot)}\right]^2}{nc} \right\}^{\frac{1}{2}} - \rho_d \sqrt{\frac{R_g T_s}{2\pi}}$$

$$\times \exp\left\{\frac{V_r^{*2}}{2R_g T_s}\right\} \Phi \left[\frac{1}{S_i \sqrt{\pi}} \left(\sqrt{\frac{T_s}{T_g}} + \frac{V_r^*}{\sqrt{2R_g T_g}} \right) \right.$$

$$\left. \left. \times \exp\left\{-\frac{V_r^*}{2R_g T_s}\right\} \right] \cdot (\boldsymbol{V}_i \cdot \hat{\boldsymbol{n}}) \right) \left[\frac{\boldsymbol{V}_i}{V_i}\right] \cdot J \, \mathrm{d}\varepsilon \, \mathrm{d}\eta$$

where

$$\rho_s = \frac{-\rho_i (\boldsymbol{V}_i \cdot \hat{\boldsymbol{n}}) - \rho_d \sqrt{(R_g T_s / 2\pi)} \exp\left\{-V_r^{*2} \big/ 2R_g T_s\right\} \Phi}{\left[\sum_{(\cdot)} \left(\boldsymbol{V}_{r_{(\cdot)}} \cdot \hat{\boldsymbol{n}}\right) \psi_{(\cdot)}\right] (1 - \Phi)}$$

$$\rho_d = \frac{-\rho_i (\boldsymbol{V}_i \cdot \hat{\boldsymbol{n}}) f_{\mathrm{ga}}}{\sqrt{(R_g T_s / 2\pi)} \exp\left\{-V_r^{*2} \big/ 2R_g T_s\right\} \Phi}, \qquad \Phi = \sum_{(\cdot)} \Phi_{(\cdot)}$$

$$(\cdot) \in \left\{ \left(\begin{matrix}\downarrow\\ \uparrow\end{matrix}\right), \left(\begin{matrix}\downarrow\\ \downarrow\end{matrix}\right), \left[\left(\begin{matrix}\downarrow\\ \downarrow\end{matrix}\right)_1 \left(\begin{matrix}\uparrow\\ \uparrow\end{matrix}\right)_2\right], \left[\left(\begin{matrix}\downarrow\\ \downarrow\end{matrix}\right)_1 \left(\begin{matrix}\downarrow\\ \uparrow\end{matrix}\right)_2\right], \left[\left(\begin{matrix}\downarrow\\ \uparrow\end{matrix}\right)_1 \left(\begin{matrix}\uparrow\\ \uparrow\end{matrix}\right)_2\right] \right\}$$

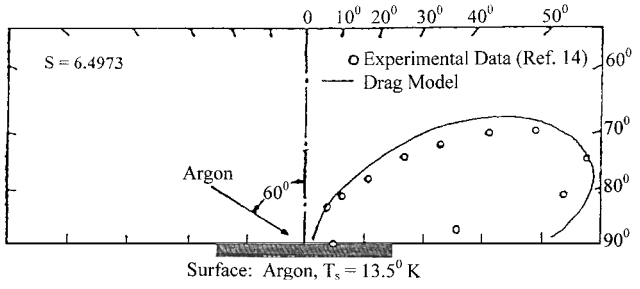

Fig. 5 In-plane spatial distribution for argon-argon gas-surface interaction.

With the unit vector $\hat{\boldsymbol{L}}$ in the direction of aerodynamic lift and the definition of $S_{\rm gn}(\hat{\boldsymbol{L}}\cdot\hat{\boldsymbol{n}})$, the lift equation for a differential surface element is given by

$$S_{\rm gn}(\hat{\boldsymbol{L}}\cdot\hat{\boldsymbol{n}}) \equiv \{+1, \hat{\boldsymbol{L}}\cdot\hat{\boldsymbol{n}} \geq 0; -1, \hat{\boldsymbol{L}}\cdot\hat{\boldsymbol{n}} < 0\}$$

$$d\boldsymbol{L} = \{-{\rm d}\dot{m}_s|\boldsymbol{V}_i/V_i \times \boldsymbol{V}_r| - {\rm d}\dot{m}_d|\boldsymbol{V}_i/V_i \times \hat{\boldsymbol{n}}(b/2)V_i|\}S_{\rm gn}(\hat{\boldsymbol{L}}\cdot\hat{\boldsymbol{n}})\hat{\boldsymbol{L}}$$

When $\boldsymbol{V}_i\cdot\hat{\boldsymbol{n}} < 0$ and $V_{r_{(\cdot)}}\cdot\psi_{(\cdot)} \leq V_i$, then

$$d\boldsymbol{L} = \left(-\rho_s\left[\sum_{(\cdot)}\left(\boldsymbol{V}_{r_{(\cdot)}}\cdot\hat{\boldsymbol{n}}\right)\psi(\cdot)\right](1-\Phi)\right.$$

$$\times\left\{\frac{\sum_{(\cdot)}\left[\left|\boldsymbol{V}_i/V_i \times \boldsymbol{V}_{r_{(\cdot)}}\right|\psi_{(\cdot)}\right]^2}{nc}\right\}^{\frac{1}{2}} - \rho_{\rm d}\sqrt{\frac{R_gT_s}{2\pi}}$$

$$\times\exp\left\{-\frac{V_r^{*2}}{2R_gT_s}\right\}\Phi\left[\frac{1}{S_i\sqrt{\pi}}\left(\sqrt{\frac{T_s}{T_g}}+\frac{V_r^*}{\sqrt{2R_gT_g}}\right)\right.$$

$$\left.\left.\times\exp\left\{-\frac{V_r^*}{\sqrt{2R_gT_s}}\right\}\right]\cdot|\boldsymbol{V}_i\times\hat{\boldsymbol{n}}|\right)S_{\rm gn}(\hat{\boldsymbol{L}}\cdot\hat{\boldsymbol{n}})\hat{\boldsymbol{L}}J\,{\rm d}\varepsilon\,{\rm d}n$$

where

$$\rho_s = \frac{-\rho_i(\boldsymbol{V}_i\cdot\hat{\boldsymbol{n}}) - \rho_d\sqrt{(R_gT_s/2\pi)}\exp\left\{-V_r^{*2}/2R_gT_s\right\}\Phi}{\left[\sum_{(\cdot)}\left(\boldsymbol{V}_{r_{(\cdot)}}\cdot\hat{\boldsymbol{n}}\right)\psi_{(\cdot)}\right](1-\Phi)}$$

$$\rho_d = \frac{-\rho_i(\boldsymbol{V}_i\cdot\hat{\boldsymbol{n}})f_{\rm ga}}{\sqrt{(R_gT_s/2\pi)}\exp\left\{-V_r^{*2}/2R_gT_s\right\}\Phi}, \qquad \Phi = \sum_{(\cdot)}\Phi_{(\cdot)}$$

$$(\cdot) \in \left\{\left(\frac{\downarrow}{\uparrow}\right), \left(\frac{\downarrow}{\downarrow}\right), \left[\left(\frac{\downarrow}{\downarrow}\right)_1\left(\frac{\uparrow}{\uparrow}\right)_2\right],\right.$$

$$\left.\left[\left(\frac{\downarrow}{\downarrow}\right)_1\left(\frac{\downarrow}{\uparrow}\right)_2\right], \left[\left(\frac{\downarrow}{\uparrow}\right)_1\left(\frac{\uparrow}{\uparrow}\right)_2\right]\right\}$$

As an example of the scattering characteristics of the drag model, we compare in Fig. 5 the drag model's in-plane spatial distribution against the experimental data for the limiting case of $\mu_g \Rightarrow 1$ for argon gas at 0.50 eV, speed ratio of 6.4973, and incidence angle of 60 deg to an argon surface at 13.5 K. The lambda collision criterion has value 476.876, and the collision scenario is XI.

Example Calculation

As an example, we evaluate the drag coefficient C_d on a cone of semivertex angle 55 deg and diameter 50 cm in a rarefied atmosphere of monatomic oxygen according to the physical conditions stipulated in the cone drag section. We use the most probable exit scattering angle $\hat{\theta}_r$ and velocity $\hat{V}_r$.

1) Monoatomic oxygen field and surface properties:

$$T_o = 300\ {\rm K}, \qquad R_o = 129.915\ {\rm J/kgK}, \qquad \mu_o = 0.28649$$

$$T_s = 100\ {\rm K}, \qquad C_{p_s} = 130\ {\rm J/kgK}, \qquad W = 0.3$$

$$M_o = 2.655748368\times10^{-26}\ {\rm kg}, \qquad \theta_i = 35\ {\rm deg}$$

$$V_i = 4187.902\ ({\rm m/s})\boldsymbol{i}, \qquad S_i = 15, \qquad \rho_i = 10^{-10}\ ({\rm kg/M^3})$$

$$R = 25\ {\rm cm}, \qquad P_{\rm ambient} = 3.9\times10^{-6}\ {\rm Pa}$$

2) Lambda and collision criteria:

$$\lambda = 905.271 - \ \text{Collision scenario IV}$$

3) Collision modes in collision scenario IV:

$$\left(\frac{\downarrow}{\uparrow}\right), \left(\frac{\downarrow}{\downarrow}\right)$$

4) Collision scenario IV probabilities:

$$\psi_{\left(\frac{\downarrow}{\uparrow}\right)} = 0.513259, \qquad \psi_{\left(\frac{\downarrow}{\downarrow}\right)} = 0.486741$$

5) Langmuir adsorption process: for the condition $r_{(\cdot)} = k_{(\cdot)}P$, we have

$$\Phi_{\left(\frac{\downarrow}{\uparrow}\right)} = \psi_{\left(\frac{\downarrow}{\uparrow}\right)}/2 = 0.2566295$$

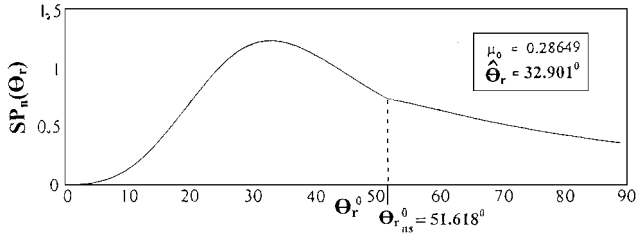

Fig. 6 Scattering probability vs exit angle for collision mode ($\frac{\downarrow}{\uparrow}$).

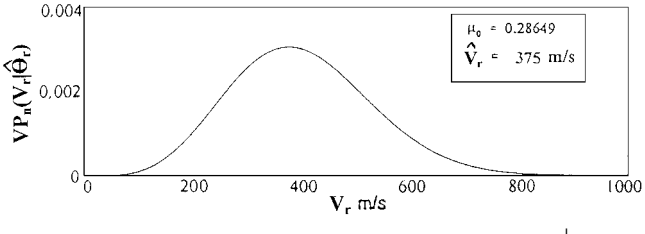

Fig. 7 Exit speed probability distribution for collision mode ($\frac{\downarrow}{\uparrow}$) at exit angle 32.901 deg.

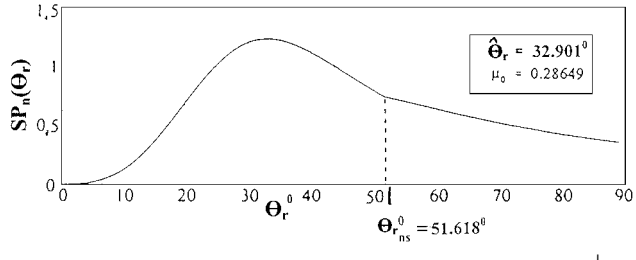

Fig. 8 Scattering probability vs exit angle for collision mode ($\frac{\downarrow}{\downarrow}$).

25.66% surface involved in adsorbing oxygen engaged in collision mode ($\downarrow\atop\downarrow$):

$$\Phi_{(\downarrow\atop\downarrow)} = \psi_{(\downarrow\atop\downarrow)}/2 = 0.2433705$$

24.34% of surface involved in adsorbing oxygen engaged in collision mode ($\downarrow\atop\uparrow$):

$$\Phi = \Phi_{(\downarrow\atop\uparrow)} + \Phi_{(\uparrow\atop\downarrow)} = 0.50 \rightarrow 50\%$$

of surface involved in gas adsorption

6) The most probable scattering exit angle $\hat{\theta}_r$ and exit scattering speed $\hat{V}_r$ are shown in Figs. 6–9 for the following collision modes:

$$\left(\frac{\downarrow}{\uparrow}\right), \left(\frac{\downarrow}{\downarrow}\right)$$

The cone drag is calculated as

$$\boldsymbol{D} = \pi R^2 \rho_i V_i \sin\theta_i \left\{ V_i - (1 - f_{\text{ga}}) \times \left[\frac{\left(\boldsymbol{V}_{r_{(\downarrow\atop\uparrow)}} \cdot \boldsymbol{i}\right)\psi_{(\downarrow\atop\uparrow)} + \left(\boldsymbol{V}_{r_{(\downarrow\atop\downarrow)}} \cdot \boldsymbol{i}\right)\psi_{(\downarrow\atop\downarrow)}}{nc} \right]^{\frac{1}{2}} - f_{\text{ga}} \left[\frac{1}{S_i\sqrt{\pi}} \left(\sqrt{\frac{T_s}{T_g}} + \frac{V_r^*}{\sqrt{2R_gT_g}} \right) \times \exp\left(-\frac{V_r^*}{\sqrt{2R_gT_s}} \right) \right] (\boldsymbol{V}_i \cdot \hat{\boldsymbol{n}}) \right\} \boldsymbol{i}$$

$$D = \pi R^2 \rho_i V_i \sin\theta_i \left(V_i - (1 - f_{\text{ga}}) \left\{ \frac{\left[\hat{V}_{r(\downarrow\atop\uparrow)} \cos\left(145 \text{ deg} - \hat{\theta}_{r(\downarrow\atop\uparrow)}\right)\psi_{(\downarrow\atop\uparrow)}\right]^2 + \left[\hat{V}_{r(\downarrow\atop\downarrow)} \cos\left(145 \text{ deg} - \hat{\theta}_{r(\downarrow\atop\downarrow)}\right)\psi_{(\downarrow\atop\downarrow)}\right]^2}{nc} \right\}^{\frac{1}{2}} + f_{\text{ga}} \left[\frac{1}{S_i\sqrt{\pi}} \left(\sqrt{\frac{T_s}{T_g}} + \frac{V_r^*}{\sqrt{2R_gT_g}} \right) \exp\left(-\frac{V_r^*}{\sqrt{2R_gT_s}} \right) \right] V_i \cos(\theta_i) \right)$$

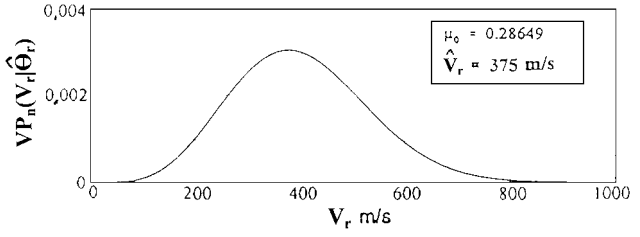

Fig. 9 Exit speed probability distribution for collision mode ($\downarrow\atop\downarrow$) at exit angle 32.901 deg.

$D = 2.28497\ \mu$N. Thus, the drag coefficient is

$$C_d = \frac{2D}{\rho_i V_i^2 \pi R^2} = 1.32705$$

Cone Drag

In Fig. 10, the behavior of the new drag model is seen for the case of computed cone drag C_d vs varying cone semivertex angle for the following gas-surface system: gas, monoatomic oxygen (O); gas constant, 129.915 J/kgK; gas temperature, 300 K; surface, iron (Fe); surface heat capacity, 130 J/kgK; surface temperature, 100 K; mass ratio of gas molecule to surface molecule, $\mu_0 = 0.28649$; and speed ratio, 15.0. The assumed data are as follows: gas density, 10^{-10} kg/m^3; ambient pressure, 3.9×10^{-6}; rotation angles α_x, α_y, 0.10 radians; surface minimum escape speed, 153.688 m/s;

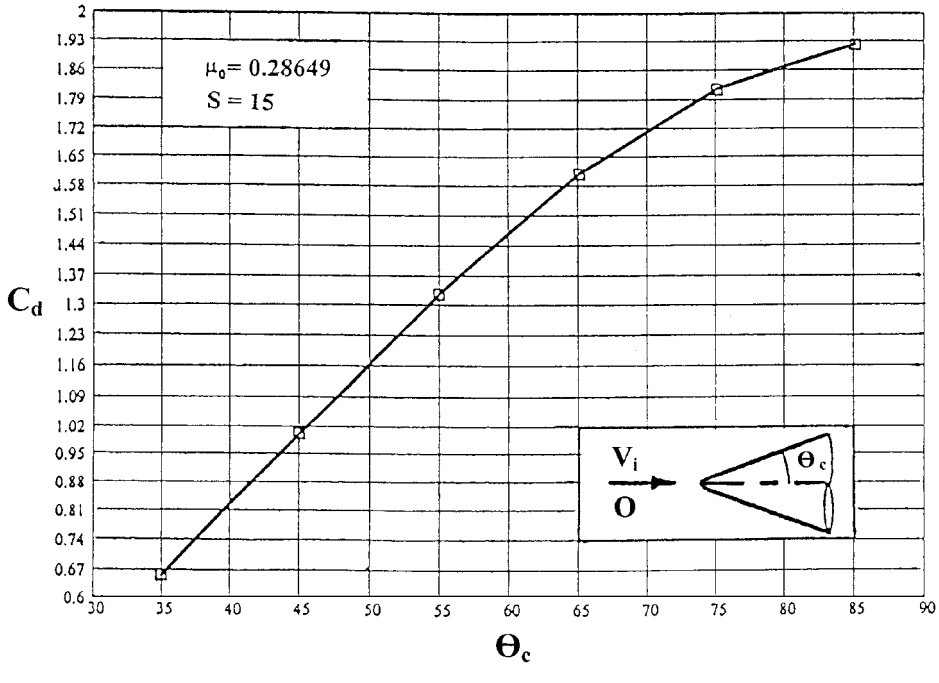

Fig. 10 Drag coefficient C_d vs cone semivertex angle θ_c.

nondimensional trapping potential well depth, 0.3; adsorbed mass fraction, 0.18834; and nondissociative adsorption, $r_{(\cdot)} = k_{(\cdot)}P$.

Conclusions

A method for the calculation of drag for convex surfaces in high-speed free molecule flow under the surface adsorption equilibrium condition has been developed. The classical hard-cube model is used to model the gas-surface scattering because of its simplicity in approximating the lobular spatial distribution scattering patterns characteristic for hyperthermal gas speeds of 100 eV or less. To the knowledge of the authors, there is no classical aerodynamic model for free molecule flow in the open literature that models the gas-surface interaction with adsorption in an explicit fashion. The classical drag model developed handles surface adsorption in an explicit fashion and is devoid of surface accommodation coefficients. In Fig. 10, the simple drag model has been implemented in Mathcad to calculate the drag coefficients of cones with semivertex angle from 35–85 deg in a monatomic oxygen gas stream at speed ratio 15; the computed drag coefficient behaves correctly by increasing with increasing cone semivertex angle.

Acknowledgments

The authors gratefully acknowledge the financial support for this research received from the Hearin Educational Enhancement Fund (No. 305726-060100-021000) at the College of Engineering, Mississippi State University. This fund was generously provided as a Grant from the Robert M. Hearin Foundation, Matt Holleman Trustee.

Appendix A: Collision Scenarios

In Tables Al–A3, We have the collision types that comprise the 12 distinct collision scenarios possible for $0 < \mu_g < 1$.

Table A1 Collision scenarios for $0 < \mu_g < \frac{1}{3}$

λ range	Collision scenarios
$(0, 1)$	I, $\left(\frac{\downarrow}{\uparrow}\right)$
$\left(1, \frac{2}{1-\mu_g}\right)$	II, $\left(\frac{\downarrow}{\uparrow}\right), \left[\left(\frac{\downarrow}{\downarrow}\right)_1 \left(\frac{\downarrow}{\uparrow}\right)_2\right]$
$\left(\frac{2}{1-\mu_g}, \frac{3-\mu_g}{1-3\mu_g}\right)$	III, $\left(\frac{\downarrow}{\uparrow}\right); \left(\frac{\downarrow}{\downarrow}\right), \left[\left(\frac{\downarrow}{\downarrow}\right)_1 \left(\frac{\uparrow}{\uparrow}\right)_2\right]$
$\left(\frac{3-\mu_g}{1-3\mu_g}, \infty\right)$	IV, $\left(\frac{\downarrow}{\uparrow}\right), \left(\frac{\downarrow}{\downarrow}\right)$

Table A2 Collision scenarios for $\frac{1}{3} < \mu_g < (5 - 2\sqrt{5})$

λ range	Collision scenarios
$(0, 1)$	V, $\left(\frac{\downarrow}{\uparrow}\right)$
$\left(1, \frac{2}{1-\mu_g}\right)$	VI, $\left(\frac{\downarrow}{\uparrow}\right), \left[\left(\frac{\downarrow}{\downarrow}\right)_1 \left(\frac{\downarrow}{\uparrow}\right)_2\right]$
$\left(\frac{2}{1-\mu_g}, \frac{3-\mu_g}{3\mu_g-1}\right)$	VII, $\left(\frac{\downarrow}{\uparrow}\right), \left(\frac{\downarrow}{\downarrow}\right), \left[\left(\frac{\downarrow}{\downarrow}\right)_1 \left(\frac{\uparrow}{\uparrow}\right)_2\right]$
$\left(\frac{3-\mu_g}{3\mu_g-1}, \infty\right)$	VIII, $\left(\frac{\downarrow}{\uparrow}\right), \left(\frac{\downarrow}{\downarrow}\right), \left[\left(\frac{\downarrow}{\uparrow}\right)_1 \left(\frac{\uparrow}{\uparrow}\right)_2\right], \left[\left(\frac{\downarrow}{\downarrow}\right)_1 \left(\frac{\uparrow}{\uparrow}\right)_2\right]$

Table A3 Collision scenarios for $(5 - 2\sqrt{5}) < \mu_g < 1$

λ range	Collision scenarios
$(0, 1)$	IX, $\left(\frac{\downarrow}{\uparrow}\right)$
$\left(1, \frac{3-\mu_g}{3\mu_g-1}\right)$	X, $\left(\frac{\downarrow}{\uparrow}\right), \left[\left(\frac{\downarrow}{\downarrow}\right)_1 \left(\frac{\downarrow}{\uparrow}\right)_2\right]$
$\left(\frac{3-\mu_g}{3\mu_g-1}, \frac{2}{1-\mu_g}\right)$	XI, $\left(\frac{\downarrow}{\uparrow}\right), \left[\left(\frac{\downarrow}{\uparrow}\right)_1 \left(\frac{\uparrow}{\uparrow}\right)_2\right], \left[\left(\frac{\downarrow}{\downarrow}\right)_1 \left(\frac{\downarrow}{\uparrow}\right)_2\right]$
$\left(\frac{2}{1-\mu_g}, \infty\right)$	XII, $\left(\frac{\downarrow}{\uparrow}\right), \left(\frac{\downarrow}{\downarrow}\right), \left[\left(\frac{\downarrow}{\uparrow}\right)_1 \left(\frac{\uparrow}{\uparrow}\right)_2\right], \left[\left(\frac{\downarrow}{\downarrow}\right)_1 \left(\frac{\uparrow}{\uparrow}\right)_2\right]$

Appendix B: Collision Types

In Tables B1 and B2, we have a description of all of the possible values of lambda criteria and phase angle for the five collision types that comprise the 12 distinct collision scenarios possible for $0 < \mu_g < 1$.

Table B1 Description of collision types for $0 < \mu_g < \frac{1}{3}$

Case	Collision type	Λ	λ
1	$\left(\frac{\downarrow}{\uparrow}\right)$	$0 < \Lambda < 2\pi$	$0 < \lambda < 1$
		$\left(\frac{V_{\text{in}} - V_s}{V_{\text{in}}}\right)\pi < \Lambda < 2\pi$	$1 < \lambda < \infty$
2	$\left[\left(\frac{\downarrow}{\downarrow}\right)_1 \left(\frac{\downarrow}{\uparrow}\right)_2\right]$	$0 < \Lambda < \left(\frac{V_{\text{in}} - V_s}{V_{\text{in}}}\right)\pi$	$1 < \lambda < \left(\frac{2}{1-\mu_g}\right)$
3	$\left(\frac{\downarrow}{\downarrow}\right)$	$0 < \Lambda < \left[\frac{(1-\mu_g)V_{\text{in}} - 2V_s}{(1+\mu_g)V_{\text{in}}}\right]2\pi$	$\left(\frac{2}{1-\mu_g}\right) < \lambda < \left(\frac{3-\mu_g}{1-3\mu_g}\right)$
4	$\left[\left(\frac{\downarrow}{\downarrow}\right)_1 \left(\frac{\uparrow}{\uparrow}\right)_2\right]$	$\left[\frac{(1-\mu_g)V_{\text{in}} - 2V_s}{(1+\mu_g)V_{\text{in}}}\right]2\pi < \Lambda < \left(\frac{V_{\text{in}} - V_s}{V_{\text{in}}}\right)\pi$	$\left(\frac{2}{1-\mu_g}\right) < \lambda < \left(\frac{3-\mu_g}{1-3\mu_g}\right)$
5	$\left(\frac{\downarrow}{\downarrow}\right)$	$0 < \Lambda < \left(\frac{V_{\text{in}} - V_s}{V_{\text{in}}}\right)\pi$	$\left(\frac{3-\mu_g}{1-3\mu_g}\right) < \lambda < \infty$

Table B2 Description of collision types for $\frac{1}{3} < \mu_g < 1$

Case	Collision type	Λ	λ
6	$\left(\frac{\downarrow}{\uparrow}\right)$	$0 < \Lambda < 2\pi$	$0 < \lambda < 1$
		$\left(\frac{V_{in} - V_s}{V_{in}}\right)\pi < \Lambda < 2\pi$	$1 < \lambda < \left(\frac{3-\mu_g}{3\mu_g - 1}\right)$
		$\left[\frac{\mu_g V_{in} - V_s}{(1+\mu_g)V_{in}}\right]4\pi < \Lambda < 2\pi$	$\left(\frac{3-\mu_g}{3\mu_g - 1}\right) < \lambda < \infty$
7	$\left[\left(\frac{\downarrow}{\uparrow}\right)_1\left(\frac{\uparrow}{\uparrow}\right)_2\right]$	$\left(\frac{V_{in} - V_s}{V_{in}}\right)\pi < \Lambda < \left[\frac{\mu_g V_{in} - V_s}{(1+\mu_g)V_{in}}\right]4\pi$	$\left(\frac{3-\mu_g}{3\mu_g - 1}\right) < \lambda < \infty$
8	$\left[\left(\frac{\downarrow}{\downarrow}\right)_1\left(\frac{\downarrow}{\uparrow}\right)_2\right]$	$0 < \Lambda < \left(\frac{V_{in} - V_s}{V_{in}}\right)\pi$	$1 < \lambda < \left(\frac{2}{1-\mu_g}\right)$
9	$\left(\frac{\downarrow}{\downarrow}\right)$	$0 < \Lambda < \left[\frac{(1-\mu_g)V_{in} - 2V_s}{(1+\mu_g)V_{in}}\right]2\pi$	$\left(\frac{2}{1-\mu_g}\right) < \lambda < \infty$
10	$\left[\left(\frac{\downarrow}{\downarrow}\right)_1\left(\frac{\uparrow}{\uparrow}\right)_2\right]$	$\left[\frac{(1-\mu_g)V_{in} - 2V_s}{(1+\mu_g)V_{in}}\right]2\pi < \Lambda < \left(\frac{V_{in} - V_s}{V_{in}}\right)\pi$	$\left(\frac{2}{1-\mu_g}\right) < \lambda < \infty$

Appendix C: Probability Distribution Factors

The component expressions $\delta_{(\cdot)}$, $\phi_{(\cdot)}$, $q_{s_{(\cdot)}}$ for each collision type that comprise the scattering probability distribution $SP_n(\theta_r)_{(\cdot)}$ and the velocity probability distribution $VP_n(V_r \mid \theta_r)_{(\cdot)}$ of the scattered gas are given next:

$$\delta = \left[1 + \left|\left(\frac{1+\mu_g}{2}\right)\frac{\cot\theta_r}{\cot\theta_i} - \left(\frac{1-\mu_g}{2}\right)\right|\right]\cdot\left|-\frac{(1+\mu_g)}{2}\frac{\csc^2\theta_r}{\cot\theta_i}\right|\cdot 4\pi$$

$$\left(\frac{\downarrow}{\uparrow}\right)\cdot\left(\frac{m_g}{2\pi k T_g}\right)^{\frac{3}{2}}\cdot\left(\frac{m_s}{2\pi k T_s}\right)^{\frac{1}{2}}\cdot\cos^{-3}\theta_i \tag{C1}$$

$$\left(\frac{\downarrow}{\uparrow}\right)\phi = \frac{m_s}{2kT_g\cos^2\theta_i} + \frac{m_s}{2kT_s}\left[\left(\frac{1+\mu_g}{2}\right)\frac{\cot\theta_r}{\cot\theta_i} - \left(\frac{1-\mu_g}{2}\right)\right]^2 \tag{C2}$$

$$\delta = \left[1 + \left|\left(\frac{1-\mu_g}{2}\right) - \left(\frac{1+\mu_g}{2}\right)\frac{\cot\theta_r}{\cot\theta_i}\right|\right]\cdot\left|\frac{(1+\mu_g)}{2}\frac{\csc^2\theta_r}{\cot\theta_i}\right|\cdot 4\pi$$

$$\left(\frac{\downarrow}{\downarrow}\right)\cdot\left(\frac{m_g}{2\pi k T_g}\right)^{\frac{3}{2}}\cdot\left(\frac{m_s}{2\pi k T_s}\right)^{\frac{1}{2}}\cdot\cos^{-3}\theta_i \tag{C3}$$

$$\left(\frac{\downarrow}{\downarrow}\right)\phi = \frac{m_g}{2kT_g\cos^2\theta_i} + \frac{m_s}{2kT_s}\left[-\left(\frac{1+\mu_g}{2}\right)\frac{\cot\theta_r}{\cot\theta_i} + \left(\frac{1-\mu_g}{2}\right)\right]^2 \tag{C4}$$

$$\left[\left(\frac{\downarrow}{\downarrow}\right)_1\left(\frac{\uparrow}{\uparrow}\right)_2\right]\left[\left(\frac{\downarrow}{\downarrow}\right)_1\left(\frac{\downarrow}{\uparrow}\right)_2\right]$$

$$\delta = \left[1 + \left|\frac{\left(1-6\mu_g+\mu_g^2\right)}{4(1-\mu_g)} + \frac{(1+\mu_g)^2}{4(1-\mu_g)}\frac{\cot\theta_r}{\cot\theta_i}\right|\right]$$

$$\times\left|\frac{-(1+\mu_g)^2}{4(1-\mu_g)}\left(\frac{\csc^2\theta_r}{\cot\theta_i}\right)\right|4\pi\left(\frac{m_g}{2\pi k T_g}\right)^{\frac{3}{2}}$$

$$\times\left(\frac{m_s}{2\pi k T_s}\right)^{\frac{1}{2}}\cdot\cos^{-3}\theta_i \tag{C5}$$

$$\phi = \frac{m_g}{2kT_g\cos^2\theta_i} + \frac{m_s}{2kT_s}\left[\frac{\left(1-6\mu_g+\mu_g^2\right)}{4(1-\mu_g)} + \frac{(1+\mu_g)^2}{4(1-\mu_g)}\frac{\cot\theta_r}{\cot\theta_i}\right]^2 \tag{C6}$$

$$\left[\left(\frac{\downarrow}{\uparrow}\right)_1\left(\frac{\uparrow}{\uparrow}\right)_2\right]$$

$$\delta = \left[1 + \left|-\frac{\left(1-6\mu_g+\mu_g^2\right)}{4(1-\mu_g)} - \frac{(1+\mu_g)^2}{4(1-\mu_g)}\frac{\cot\theta_r}{\cot\theta_i}\right|\right]$$

$$\times\left|\frac{(1+\mu_g)^2}{4(1-\mu_g)}\left(\frac{\csc^2\theta_r}{\cot\theta_i}\right)\right|\cdot 4\pi\left(\frac{m_g}{2\pi k T_g}\right)^{\frac{3}{2}}$$

$$\times\left(\frac{m_s}{2\pi k T_s}\right)^{\frac{1}{2}}\cdot\cos^{-3}\theta_i \tag{C7}$$

$$\phi = \frac{m_g}{2kT_g\cos^2\theta_i} + \frac{m_s}{2kT_s}\left[-\frac{\left(1-6\mu_g+\mu_g^2\right)}{4(1-\mu_g)} - \frac{(1+\mu_g)^2}{4(1-\mu_g)}\frac{\cot\theta_r}{\cot\theta_i}\right]^2 \tag{C8}$$

$$\left(\frac{\downarrow}{\uparrow}\right)\quad q_s = q_r\left[\left(\frac{1+\mu_g}{2}\right)\cos\theta_r - \left(\frac{1-\mu_g}{2}\right)\sin\theta_r\cot\theta_i\right] \tag{C9}$$

$$\left(\frac{\downarrow}{\downarrow}\right)\quad q_s = q_r\left[-\left(\frac{1+\mu_g}{2}\right)\cos\theta_r + \left(\frac{1-\mu_g}{2}\right)\sin\theta_r\cot\theta_i\right] \tag{C10}$$

$$\left[\left(\frac{\downarrow}{\downarrow}\right)_1\left(\frac{\uparrow}{\uparrow}\right)_2\right]\left[\left(\frac{\downarrow}{\downarrow}\right)_1\left(\frac{\downarrow}{\uparrow}\right)_2\right]$$

$$q_s = q_r\left[\frac{\left(1-6\mu_g+\mu_g^2\right)}{4(1-\mu_g)}\sin\theta_r\cot\theta_i + \frac{(1+\mu_g)^2}{4(1-\mu_g)}\cos\theta_r\right] \tag{C11}$$

$$\left[\left(\frac{\downarrow}{\uparrow}\right)_1\left(\frac{\uparrow}{\uparrow}\right)_2\right]$$

$$q_s = q_r\left[-\frac{\left(1-6\mu_g+\mu_g^2\right)}{4(1-\mu_g)}\sin\theta_r\cot\theta_i - \frac{(1+\mu_g)^2}{4(1-\mu_g)}\cos\theta_r\right] \tag{C12}$$

References

[1]Maxwell, J. C., "On the Dynamical Theory of Gases," *Philosophical Transactions of the Royal Society of London*, Vol. 157, 1867, pp. 49–88.

[2]Devienne, P. M., Souquet, J., and Rousten, J. C., "Study of the Scattering of High Energy Molecules by Various Surfaces," *Fourth International Symposium on Rarefied Gas Dynamics*, edited by J. H. de Leeuw, Vol. 2, Academic Press, New York, 1966, pp. 584–594.

[3]Goodman, F. O., "On the Theory of Accommodation Coefficients—IV. Simple Distribution Function Theory of Gas-Solid Interaction Systems," *Journal of Physics and Chemistry of Solids*, Vol. 26, 1965, pp. 85–105.

[4]Logan, R. M., and Stickney, R. E., "Simple Classical Model for the Scattering of Gas Atoms from a Solid Surface," *The Journal of Chemical Physics*, Vol. 44, Jan. 1966, pp. 195–201.

[5]Logan, R. M., Keck, R. M., and Stickney, R. E., "Simple Classical Model for the Scattering of Gas Atoms from a Solid Surface: Additional Analysis and Comparisons," *Rarefied Gas Dynamics*, Vol. 1, Academic Press, New York, 1967, pp. 49–66.

[6]Busby, M. R., Haygood, J. D., and Link, C. H. Jr., "Classical Model for Gas-Surface Interaction," *The Journal of Chemical Physics*, Vol. 54, No. 11, 1971, pp. 4642–4647.

[7]Hudson, J. B., *Surface Science: An Introduction*, Wiley, New York, 1998, pp. 128, 152, 171, 178.

[8]Belena, J. F., "Drag Model for Convex Surfaces in High Speed Free Molecule Flow," Ph.D. Dissertation, Dept. of Aerospace Engineering, Mississippi State Univ., 2000, pp. l–l80.

[9]Carter, W. J., "Optimum Nose Shapes for Missiles in the Superaerodynamic Region," *Journal of the Aeronautical Sciences*, Vol. 27, No. 7, 1957, pp. 527–532.

[10]Hayward, D. O., and Trapnell, B. M. W., *Chemisorption*, Academic Press, New York, 1964.

[11]Crowell, A. D., *The Solid-Gas Interface 1*, Marcel Dekker, Inc., New York, 1967, Chap. 7, pp. 175–201.

[12]Warsi, Z. U. A., and Belena, J. F., "Effect of Catalytic Surface Curvature on the Chemical Performance with Defect Structures," *Chemical Engineering Journal* (to be published).

[13]Langmuir, I. J., *Journal American Chemical Society*, Vol. 4, No. 2, 1918, pp. 1361–1403.